

Large Unidirectional Magnetoresistance in a Magnetic Topological Insulator

K. Yasuda,^{1,*} A. Tsukazaki,² R. Yoshimi,³ K. S. Takahashi,³ M. Kawasaki,^{1,3} and Y. Tokura^{1,3}

¹*Department of Applied Physics and Quantum-Phase Electronics Center (QPEC), University of Tokyo, Tokyo 113-8656, Japan*

²*Institute for Materials Research, Tohoku University, Sendai 980-8577, Japan*

³*RIKEN Center for Emergent Matter Science (CEMS), Wako 351-0198, Japan*

(Dated: September 21, 2016)

We report current-direction dependent or unidirectional magnetoresistance (UMR) in magnetic/nonmagnetic topological insulator (TI) heterostructures, $\text{Cr}_x(\text{Bi}_{1-y}\text{Sb}_y)_{2-x}\text{Te}_3/(\text{Bi}_{1-y}\text{Sb}_y)_2\text{Te}_3$, that is several orders of magnitude larger than in other reported systems. From the magnetic field and temperature dependence, the UMR is identified to originate from the asymmetric scattering of electrons by magnons. In particular, the large magnitude of UMR is an outcome of spin-momentum locking and a small Fermi wavenumber at the surface of TI. In fact, the UMR is maximized around the Dirac point with the minimal Fermi wavenumber.

PACS numbers: 72.10.Di, 72.25.-b, 75.47.-m, 75.76.+j

Transfer and conservation of angular momentum is at the heart of spintronics [1–5]; spin transfer torque works to convert spin-polarized current to and from magnons, thus enabling the electrical control of magnetism. For example, current induced magnetization reversal and spin torque ferromagnetic resonance through spin injection have been realized in various heterostructures based on heavy metal element (with large spin-orbit coupling) and ferromagnet, such as Pt/Py, Ta/CoFeB and Pt/Co [2–5]. Recently, it has been reported that unidirectional magnetoresistance (UMR) emerges in such heterostructures under in-plane magnetization [6–8]; the resistance value is different depending on the sign of the outer product of current J and magnetization M vectors. There, the spin accumulation direction, either parallel or anti-parallel with M , at the interface by spin Hall effect has been proposed to be a major origin of UMR [6–8], in analogy to the giant magnetoresistance (GMR) effect [9, 10], which depends on the relationship of magnetizations, parallel or antiparallel, in stacked ferromagnetic metal layers. In a broader context, the UMR is expected to be further enhanced in topological insulator (TI) with large spin Hall angle [11–14] via spin-momentum locking (Fig. 1(a)), because the spin polarization at the surface would govern the amplitude of this effect.

In this study, we investigate the UMR of TI heterostructures [12, 15, 16] composed of nonmagnetic TI $(\text{Bi}_{1-y}\text{Sb}_y)_2\text{Te}_3$ (BST) [17, 18] and magnetic TI $\text{Cr}_x(\text{Bi}_{1-y}\text{Sb}_y)_{2-x}\text{Te}_3$ (CBST) [19] on insulating InP substrate. By tuning the composition y , we could control the Fermi energy E_F of the surface state inside the bulk band gap, which is confirmed by the Hall effect measurement [15–18]. Here, the main players of conduction are top and bottom surfaces with single Dirac cones around the Γ point [15, 16, 20, 21]. In addition, in the heterostructure, only one surface involved in the Cr-doped layer effectively interacts with magnetism [15, 16]. Thus, in terms of the symmetry consideration of spin-

momentum locking (Fig. 1(a)), we can expect that magnetoresistance depends on the relative configuration between surface electron spin and M directions; parallel (Fig. 1(b)) or antiparallel (Fig. 1(c)).

Thin films of TI heterostructures were grown with molecular beam epitaxy in the same procedures as described in Refs. [15] and [16]. The nominal compositions of TI heterostructure $\text{Cr}_x(\text{Bi}_{1-y}\text{Sb}_y)_{2-x}\text{Te}_3/(\text{Bi}_{1-y}\text{Sb}_y)_2\text{Te}_3$ are $x \sim 0.2$ and $y \sim 0.86$. Using photolithography and Ar ion milling, thin films were patterned into the shape of Hall bar, 10 μm in width and 36 μm in length. After that, the electrodes Au (45 nm)/Ti (5 nm) were formed by electron beam deposition [22]. The transport measurements were performed mainly at 2 K in Physical Property Measurement System (Quantum Design) using dc current source and a voltmeter.

Figure 1(e) shows the measured magnetoresistance of the heterostructure CBST (3 nm)/BST (5 nm) (Fig. 1(d)). First, we notice that resistance decreases with increasing in-plane magnetic field B . Because of the out-of-plane anisotropy of M in CBST, M initially points along the z -direction forming the exchange gap in surface Dirac state. As magnetic field is applied up to 0.7 T, the magnetization direction gradually changes to the in-plane so that the eventual gap closing of the Dirac surface state causes negative magnetoresistance [22]. Also, we note that the resistance measured under $+1 \mu\text{A}$ (red) and $-1 \mu\text{A}$ (blue) at 2 K show a noticeable deviation as shown in Fig. 1(e); the difference ΔR_{xx} between the two current directions is plotted in Fig. 1(f). Here, ΔR_{xx} is anti-symmetrized as a function of B and M . ΔR_{xx} is initially almost zero at 0 T where M is pointing out-of-plane, and then increases as the field increases up to 0.7 T. At higher magnetic field above 0.7 T, ΔR_{xx} becomes almost constant, whose sign is reversed in accordance with M reversal in CBST. Furthermore, ΔR_{xx} is also reversed in sign, as shown in Figs. 1(h) and 1(i),

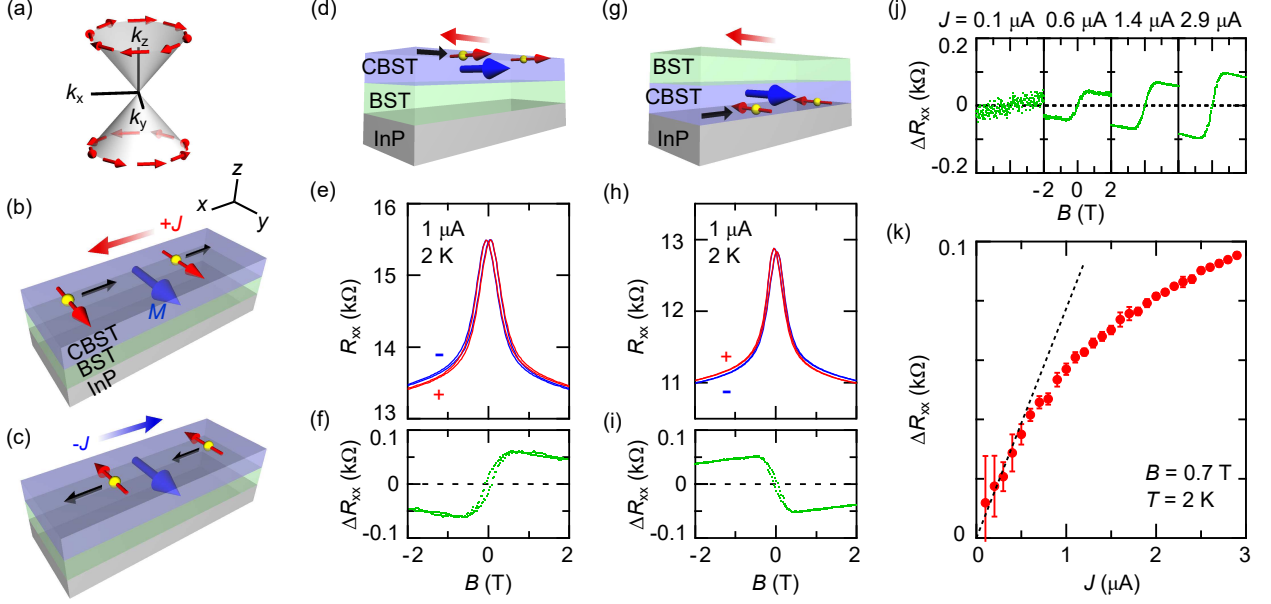


FIG. 1. (color online) (a) Schematic diagram of spin-momentum locking of surface Dirac state in TI. (b), (c) Schematic illustration of the concept for UMR in TI heterostructures $\text{Cr}_x(\text{Bi}_{1-y}\text{Sb}_y)_{2-x}\text{Te}_3/(\text{Bi}_{1-y}\text{Sb}_y)_2\text{Te}_3$ (CBST/BST) on InP substrate under $+J$ (b) and $-J$ (c) dc current. Here, magnetic field, magnetization and dc current are along the in-plane direction, where dc current is applied perpendicular to the magnetization direction. (d) Schematic illustration of a “normal” CBST/BST heterostructure. (e) Magnetic field dependence of resistance R_{xx} for the sample depicted in (d) measured under $J = +1 \mu\text{A}$ (red) and $J = -1 \mu\text{A}$ (blue) at 2 K. (f), Difference of the resistance ΔR_{xx} of plus and minus current shown in (e). (g)-(i) The same as (d)-(f) for the “inverted” BST/CBST heterostructure. (j) ΔR_{xx} measured under various current for the normal CBST/BST heterostructure. (k) Current J dependence of ΔR_{xx} at 2 K under $B = 0.7 \text{ T}$ for the normal CBST/BST. The black dotted line shows a slope in the low- J region.

for the inverted heterostructure BST (3 nm)/CBST (5 nm) (Fig. 1(g)), while showing the similar absolute magnitude of UMR. This is most likely because the manner of the spin-momentum locking is opposite between the top and bottom surfaces as depicted in Figs. 1(d) and 1(g). This leads to the cancellation of UMR in the case of the single-layer CBST film [22]. Figures 1(j) and 1(k) show the current amplitude dependence of UMR. While ΔR_{xx} shows a negligibly small difference with current amplitude of $0.1 \mu\text{A}$, it is progressively enhanced with increasing current. The current J dependence of ΔR_{xx} at 0.7 T is summarized in Fig. 1(k), which shows a linear relationship in a low current region, typically $J < 0.5 \mu\text{A}$. Therefore, the relationship between electric field E_x and current density j_x should be expressed in a nonlinear form in such a low current region,

$$E_x = R_{xx}j_x + R_{xx}^{(2)}j_x^2. \quad (1)$$

Here, $\Delta R_{xx} = 2R_{xx}^{(2)}j_x$ is linearly proportional to current density. The derivation from the linear relationship in Fig. 1(k) at high current ($> 0.5 \mu\text{A}$) is attributed to heating effect by fairly large current excitation, up to $\Delta T = 2.3 \text{ K}$ at $J = 3 \mu\text{A}$ as estimated from the change of R_{xx} [22]. Hereafter, we applied $\pm 1 \mu\text{A}$ for the measurements to get enough S/N ratio but to make the heating effect

as small as possible.

In Table I, we compare the magnitude of UMR in the present device with those of previously reported heterostructures [6–8]. Since it is linear in current, we adopt the quantity $(\Delta R_{xx}/R_{xx})/j$ as a measure of UMR for a fair comparison. In the TI heterostructure, we define the current density by considering each surface conduction thickness of $\sim 1 \text{ nm}$ [24] (see also the legend of Table 1). Even though the current density is much smaller than other systems, $\Delta R_{xx}/R_{xx}$ is comparable or larger. Therefore, the amplitude of $(\Delta R_{xx}/R_{xx})/j$ is quite large, $10^2 - 10^6$ times larger than other bilayer systems, *e.g.* GaMnAs heterostructure or Pt/Co [6–8].

To elucidate a possible origin of such a large UMR, we investigated angular dependence of the signal. Figures 2(b) and 2(c) show the in-plane magnetic-field directional dependence of normalized ΔR_{xx} and M_y ($\propto \cos \varphi$); here definition of azimuth angle φ is shown in Fig. 2(a). The $|\Delta R_{xx}|$ is largest at $B \parallel y\text{-axis}$ ($\varphi = 0^\circ, 180^\circ$ and 360°), scaling well with the $\cos \varphi$ dependence of M_y . Figures 2(e) and 2(f) show the out-of-plane magnetic-field directional dependence of normalized ΔR_{xx} (see Fig. 2(d)). Here, M_y and M_z are estimated from the variation of anomalous Hall effect. In accord with the in-plane case, the $|\Delta R_{xx}|$ is largest at $B \parallel y\text{-axis}$ ($\theta = -90^\circ, 90^\circ$). It

TABLE I. Comparison of UMR magnitude for various heterostructures. Note that the values marked with asterisk * for CBST/BST are calculated with assuming the thickness of conductive region ~ 2 nm of top and bottom surface states [24]. Even if the total thickness of the whole film (~ 8 nm) were taken, the values would be changed only by a factor of four.

Material	j (A/cm ²)	R_{xx} (Ω)	ΔR_{xx} (Ω)	$\Delta R_{xx}/R_{xx}$ (%)	$\Delta R_{xx}/R_{xx}/j$ (arb.units)
Ta/Co [7]	10^7	574	0.011	0.0019	1.3
Pt/Co [7]	10^7	176	0.0025	0.0014	1
GaMnAs heterostructure [6]	7.5×10^5	1720	2	0.12	1.1×10^3
CBST/BST (this study)	5.0×10^3 *	14000	57	0.41	5.7×10^5 *

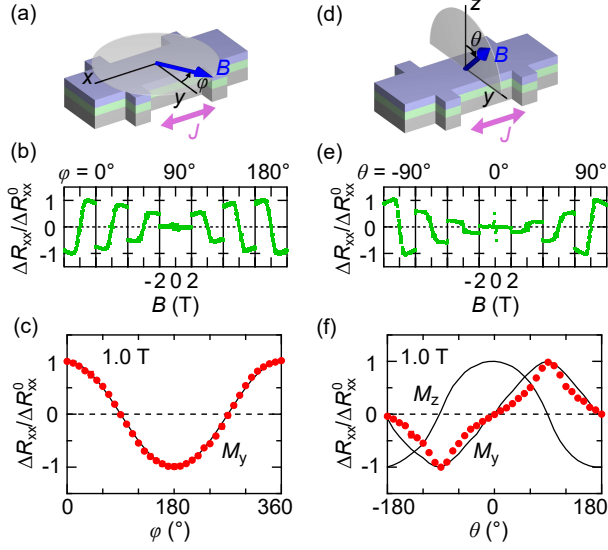


FIG. 2. (color online) (a) Schematic sample configuration for the measurement of in-plane magnetic field φ dependence of ΔR_{xx} . φ is measured from y -axis. (b), (c) Magnetic field and φ dependence (by 30° step) of normalized ΔR_{xx} , $\Delta R_{xx}/\Delta R_{xx}^0$. Here, ΔR_{xx}^0 is ΔR_{xx} at $\varphi = 0^\circ$ and 1.0 T. (d)-(f) The same as (a)-(c) for the out-of-plane magnetic field θ dependence. θ is measured from z -axis. Here, ΔR_{xx}^0 is ΔR_{xx} at $\theta = 90^\circ$ and 1.0 T.

is noticeable, however, that the ΔR_{xx} does not simply scale with M_y . This is perhaps because the finite M_z component makes the Dirac dispersion massive, which effectively weakens the spin-momentum locking [25]. To summarize, UMR emerges only when M_y component is finite.

One possible origin of such nonlinear magnetoresistance might be an additional voltage caused by heat gradient along z -direction such as anomalous Nernst effect and spin Seebeck effect [26–28]. In both processes, induced voltage would be expressed as $V_{\text{thermal}} \propto M \times (\nabla T)_z$ [26–28], so that finite M_y component might cause an additional voltage along the x -direction. However, we can safely exclude this possibility since the additional voltage should exhibit the same sign for the both heterostructures of CBST/BST/InP (Fig. 1(d)) and BST/CBST/InP (Fig. 1(g)) when InP works as a heat bath; this is inconsistent with the experimentally ob-

served opposite sign shown in Figs. 1(f) and 1(i). Therefore, the origin of UMR should be explored in intrinsic scattering mechanisms related to electron spins. To clarify the microscopic origin, we studied the temperature dependence under higher magnetic field (Fig. 3(a)). UMR at low magnetic field decreases with increasing temperatures until it almost vanishes at around Curie temperature $T_C \sim 24$ K [22], confirming its close relevance to the ferromagnetic magnetization. This is also evident from the absence of UMR within the present experimental error in the single-layer BST film [22]. On the other hand, UMR is strongly suppressed at high magnetic field, meaning that it does not simply scale with M_y . This indicates that the UMR in TI cannot be explained in terms of the GMR mechanism that was proposed for the case of ferromagnet/normal metal bilayers [6–8]. Rather, such a field induced suppression of $|\Delta R_{xx}|$ is reminiscent of the cases of Spin Seebeck effect [27, 28] and magnon Hall effect [29], in which the magnon population and hence the signal magnitude are suppressed by gap opening of spin wave (magnon) at higher field. This leads us to consider the scattering of surface Dirac electrons by magnons as a microscopic origin of UMR.

With spin-momentum locking, conservation of angular momentum leads to the one-way scattering by magnon: Taking the quantization direction along $M||y$ -axis, the angular momentum of magnon is $+1$ (note that spin angular momentum points opposite to M). Thus, as shown in Fig. 3(b), when electron with $s_y = -1/2$ spin (left branch) is back-scattered to $s_y = 1/2$ (right branch), the electron absorbs magnon because of the conservation of angular momentum. On the other hand, when it goes from $s_y = 1/2$ to $s_y = -1/2$, it emits magnon as a reverse process. Phenomena related to such a transfer of angular momentum between electron spin and magnetization has been widely recognized in the field of spintronics [1]; for example, spin Seebeck effect [26–28], spin Peltier effect [30], spin pumping [31, 32] and spin torque ferromagnetic resonance [2, 3, 13, 14]. In such a scattering process by magnon, we can derive the formula of UMR by Boltzmann transport equation with the relaxation time approximation [33] as follows (see Supplemental Material

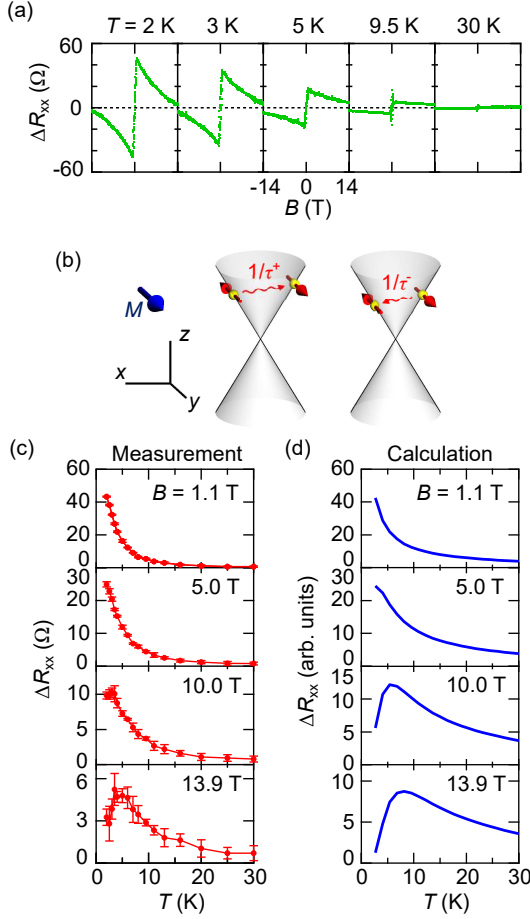


FIG. 3. (color online) (a) Magnetic field dependence of ΔR_{xx} at various temperatures. (b) Schematic concepts of asymmetric scattering of spin-polarized surface Dirac electron by magnon. (c) Temperature dependence of ΔR_{xx} under various magnetic fields. (d) Numerical calculation results of temperature dependent ΔR_{xx} under various magnetic fields.

[22]);

$$\Delta R_{xx} \propto j_x \int k_x \left(-\frac{1}{\tau^+} + \frac{1}{\tau^-} \right) \left(\frac{\partial^2 f}{\partial E^2} \right), \quad (2)$$

$$\frac{1}{\tau^+} \propto \frac{1}{e^{\beta \hbar \omega} - 1} \left(1 - \frac{1}{e^{\beta(\hbar \omega + \hbar v_F k_x - E_F)} + 1} \right), \quad (3)$$

$$\frac{1}{\tau^-} \propto \left(\frac{1}{e^{\beta \hbar \omega} - 1} + 1 \right) \left(1 - \frac{1}{e^{\beta(-\hbar \omega + \hbar v_F k_x - E_F)} + 1} \right). \quad (4)$$

Here, f is the Fermi distribution function and $\hbar \omega$ is the magnon energy with wavenumber $\sim 2k_F$ (k_F : Fermi wavenumber). τ^+ (τ^-) is relaxation time of magnon scattering from left(right) branch to right (left) one. The first factors of equations (3) and (4) are the probability of magnon absorption and emission, respectively, and the second ones are the probability that the final state of electron is unoccupied. Since $1/\tau^+$ and $1/\tau^-$ are not equal in general, equation (2) gives finite UMR in TI. Note

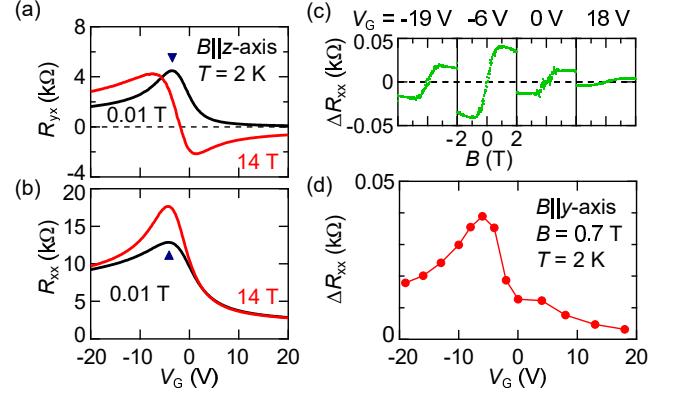


FIG. 4. (color online) (a), (b) Gate voltage V_G dependence of Hall resistance (R_{yx}) and longitudinal resistance (R_{xx}) under magnetic field $B(\parallel z)$ of 0.01 T and 14 T at 2 K. (c), (d) Magnetic field and V_G dependence of ΔR_{xx} . The ΔR_{xx} is taken at $B(\parallel y) = 0.7$ T.

that equation (2) is derived for the one-dimensional (1D) Dirac dispersion but this can be readily extended to the actual 2D case without essential change of the scheme [22].

Figures 3(c) and 3(d) display the comparison of experimental results of the temperature and magnetic-field dependence of UMR with the calculated ones based on the above model assuming the magnon energy of $g\mu_B B$ [34] with $g \sim 2$ for the localized Cr moment in CBST. Both results give qualitative consistency; the UMR monotonically increases with decreasing temperature at low magnetic field (1.1 T and 5.0 T), while the magnon gap as large as ~ 20 K opens at 13.9 T so that the UMR takes a peak structure around the temperature comparable with the magnon gap. Here, the deviation of numerical calculation from experimental result above 10 K originates from the breakdown of the adopted spin wave approximation [22] at temperatures close to $T_C \sim 24$ K. This microscopic model helps us to understand why the UMR in TI is so large: One reason is the spin-momentum locking inherent in TI. Unlike the Rashba interface with two bands having opposite spin helicity, TI with single spin-momentum locking can accumulate spin efficiently without cancellation. Another factor is that TI with tuned E_F around the Dirac point can have a small Fermi momentum k_F lower than $\sim 500 \mu\text{m}^{-1}$ [17, 18]. Therefore, magnons with small wavenumber and low energy can dominantly contribute to electron scattering, which is easily populated even at low temperatures.

Finally, we discuss the E_F dependence of UMR in the field-effect transistor of TI heterostructure. Here, AlOx layer with a thickness of 30 nm was deposited as a top gate dielectric. Figures 4(a) and 4(b) show the gate voltage V_G dependence of R_{yx} and R_{xx} under $B(\parallel z)$ -axis at 0.01 T and 14 T. Anomalous Hall effect (R_{yx} measured at 0.01 T, shown by a black line in Fig. 4(a)) and R_{xx} (Fig.

4(b)) take maxima at around -4 V, indicating that E_F of the top surface state is tuned close to the Dirac point [15]. The V_G dependence of UMR measured under $B||y$ -axis is summarized in Figs. 4(c) and 4(d). To exclude the V_G dependence of relaxation time (denoted as $\tau^{(0)}$ in Supplemental Material), we plot ΔR_{xx} , not $\Delta R_{xx}/R_{xx}$, in Fig. 4(d) [22]. First, the sign of ΔR_{xx} does not change with V_G , *i.e.* irrespective of E_F position in hole ($V_G = -19$ V) and electron ($V_G = 0$ V and 18 V) doping regions. This can be understood by considering the scattering process for the hole side in the same way as shown in Fig. 3(b) for the electron side [22]. Moreover, the UMR is maximized at E_F being close to the Dirac point ($V_G = -6$ V). As k_F decreases with E_F approaching the Dirac point, the wavenumber and energy of magnon contributing to the scattering process decrease so that related magnon population increases. This, in combination with the decrease of k_F , results in the maximum ΔR_{xx} and UMR with E_F around the Dirac point.

To summarize, we observed UMR in magnetic TI, which is shown to be several orders of magnitude larger than in other reported systems [6–8]. The origin of UMR is identified to be the asymmetric scattering of electrons by magnons. Improvement of theoretical calculation [22] and understanding of the relationship with spin-orbit torque remain as future issues [12–14].

We thank T. Yokouchi, T. Ideue, Y. Okamura, N. Ogawa, S. Seki, K. Hamamoto and N. Nagaosa for fruitful discussions, and S. Shimizu for experimental support. This research was supported by the Japan Society for the Promotion of Science through the Funding Program for World-Leading Innovative R & D on Science and Technology (FIRST Program) on “Quantum Science on Strong Correlation” initiated by the Council for Science and Technology Policy and by JSPS Grant-in-Aid for Scientific Research(S) No. 24224009 and No. 24226002 from MEXT, Japan.

* yasuda@cmr.t.u-tokyo.ac.jp

- [1] A. V. Chumak, V. I. Vasyuchka, A. A. Serga, and B. Hillebrands, *Nat. Phys.* **11**, 453 (2015).
- [2] L. Liu, T. Moriyama, D. C. Ralph, and R. A. Buhrman, *Phys. Rev. Lett.* **106**, 036601 (2011).
- [3] L. Liu, C. F. Pai, Y. Li, H. W. Tseng, D. C. Ralph, and R. A. Buhrman, *Science* **336**, 555 (2012).
- [4] I. M. Miron, K. Garello, G. Gaudin, P. J. Zermatten, M. V. Costache, S. Auffret, S. Bandiera, B. Rodmacq, A. Schuhl, and P. Gambardella, *Nature (London)* **476**, 189 (2011).
- [5] L. Liu, O. J. Lee, T. J. Gudmundsen, D. C. Ralph, and R. A. Buhrman, *Phys. Rev. Lett.* **109**, 096602 (2012).
- [6] K. Olejník, V. Novák, J. Wunderlich, and T. Jungwirth, *Phys. Rev. B* **91**, 180402 (2015).
- [7] C. O. Avci, K. Garello, A. Ghosh, M. Gabureac, S. F. Alvarado, and P. Gambardella, *Nat. Phys.* **11**, 570 (2015).
- [8] C. O. Avci, K. Garello, J. Mendil, A. Ghosh, N. Blasakis, M. Gabureac, M. Trassin, M. Fiebig, and P. Gambardella, *Appl. Phys. Lett.* **107**, 192405 (2015).
- [9] M. N. Baibich, J. M. Broto, A. Fert, F. Nguyen Van Dau, F. Petroff, P. Etienne, G. Creuzet, A. Friederich, and J. Chazelas, *Phys. Rev. Lett.* **61**, 2472 (1988).
- [10] G. Binasch, P. Grünberg, F. Saurenbach, and W. Zinn, *Phys. Rev. B* **39**, 4828 (1989).
- [11] M. Z. Hasan, and C. L. Kane, *Rev. Mod. Phys.* **82**, 3045 (2010).
- [12] Y. Fan *et al.*, *Nat. Mater.* **13**, 699 (2014).
- [13] A. R. Mellnik *et al.*, *Nature (London)* **511**, 449 (2014).
- [14] K. Kondou, R. Yoshimi, A. Tsukazaki, Y. Fukuma, J. Matsuno, K. S. Takahashi, M. Kawasaki, Y. Tokura, Y. Otani, Preprint (2015). arXiv:1510.03572.
- [15] R. Yoshimi, K. Yasuda, A. Tsukazaki, K. S. Takahashi, N. Nagaosa, M. Kawasaki, and Y. Tokura, *Nat. Commun.* **6**, 8530 (2015).
- [16] K. Yasuda, R. Wakatsuki, T. Morimoto, R. Yoshimi, A. Tsukazaki, K. S. Takahashi, M. Ezawa, M. Kawasaki, N. Nagaosa, and Y. Tokura, *Nat. Phys.* **12**, 555 (2016).
- [17] J. Zhang *et al.*, *Nat. Commun.* **2**, 574 (2011).
- [18] R. Yoshimi, A. Tsukazaki, Y. Kozuka, J. Falson, K. S. Takahashi, J. G. Checkelsky, N. Nagaosa, M. Kawasaki, and Y. Tokura, *Nat. Commun.* **6**, 6627 (2015).
- [19] C. Z. Chang *et al.*, *Adv. Mater.* **25**, 1065 (2013).
- [20] H. Zhang, C. X. Liu, X. L. Qi, X. Dai, Z. Fang, and S. C. Zhang, *Nat. Phys.* **5**, 438 (2009).
- [21] Y. Xia *et al.*, *Nat. Phys.* **5**, 398 (2009).
- [22] See Supplemental Material, which includes Refs. [20, 23, 33], for additional information and a detailed theoretical derivation of UMR.
- [23] T. Holstein, and H. Primakoff, *Phys. Rev.* **58**, 1098 (1940).
- [24] Y. Zhang *et al.*, *Nat. Phys.* **6**, 584 (2010).
- [25] S. Y. Xu *et al.*, *Nat. Phys.* **8**, 616 (2012).
- [26] K. Uchida, H. Adachi, T. Ota, H. Nakayama, S. Maekawa, and E. Saitoh, *Appl. Phys. Lett.* **97**, 172505 (2010).
- [27] T. Kikkawa, K. Uchida, Y. Shiomi, Z. Qiu, D. Hou, D. Tian, H. Nakayama, X.-F. Jin, and E. Saitoh, *Phys. Rev. Lett.* **110**, 067207 (2013).
- [28] T. Kikkawa, K. I. Uchida, S. Daimon, Z. Qiu, Y. Shiomi, and E. Saitoh, *Phys. Rev. B* **92**, 064413 (2015).
- [29] Y. Onose, T. Ideue, H. Katsura, Y. Shiomi, N. Nagaosa, and Y. Tokura, *Science* **329**, 297 (2010).
- [30] J. Flipse, F. K. Dejene, D. Wagenaar, G. E. W. Bauer, J. B. Youssef, and B. J. vanWees, *Phys. Rev. Lett.* **113**, 027601 (2014).
- [31] E. Saitoh, M. Ueda, H. Miyajima, and G. Tatara, *Appl. Phys. Lett.* **88**, 182509 (2006).
- [32] Y. Shiomi, K. Nomura, Y. Kajiwara, K. Eto, M. Novak, K. Segawa, Y. Ando, and E. Saitoh, *Phys. Rev. Lett.* **113**, 196601 (2014).
- [33] N. W. Ashcroft, and N. D. Mermin, *Solid State Physics* (Saunders College, 1976).
- [34] G. V. Skrotskii, and L. V. Kurbatov, *Ferromagnetic Resonance* (Pergamon, 1966).

Supplemental Material for Large Unidirectional Magnetoresistance in a Magnetic Topological Insulator

SUPPLEMENTAL MATERIAL S1 | DEVICE STRUCTURE

Figure S1 shows the top view of the device structure. The size of the Hall bar is $10\ \mu\text{m}$ in width and $36\ \mu\text{m}$ in length, respectively.

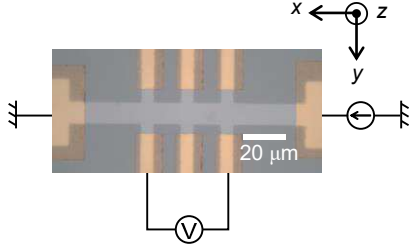


Fig. S1. top view of the device structure.

SUPPLEMENTAL MATERIAL S2 | MAGNETIC ANISOTROPY AND BAND STRUCTURE

$\text{Cr}_x(\text{Bi}_{1-y}\text{Sb}_y)_{2-x}\text{Te}_3$ shows a perpendicular magnetic anisotropy. Thus, M is pointing along z -direction at 0 T with the coercive field of ~ 0.1 T (Fig. S2(a)). On the other hand, M is directed to in-plane when the in-plane magnetic field of ~ 0.7 T is applied (Fig. S2(b)). Because of the coupling between electron spin and localized moment, the Hamiltonian of surface electron is affected by the direction of magnetization M . The original Hamiltonian without M is expressed as,

$$H = \alpha(k_y\sigma_x - k_x\sigma_y), \quad (\text{S1})$$

as displayed in Fig. S2(c). With the out-of-plane $M||z$, it turns to

$$H = \alpha(k_y\sigma_x - k_x\sigma_y) + m\sigma_z, \quad (\text{S2})$$

so that the Dirac dispersion gets massive (Fig. S2(d)). On the other hand, with the in-plane $M||y$, it turns to

$$H = \alpha k_y\sigma_x + (m - \alpha k_x)\sigma_y, \quad (\text{S3})$$

which shifts the gapless Dirac cone to the k_x -direction (Fig. S2(e)).

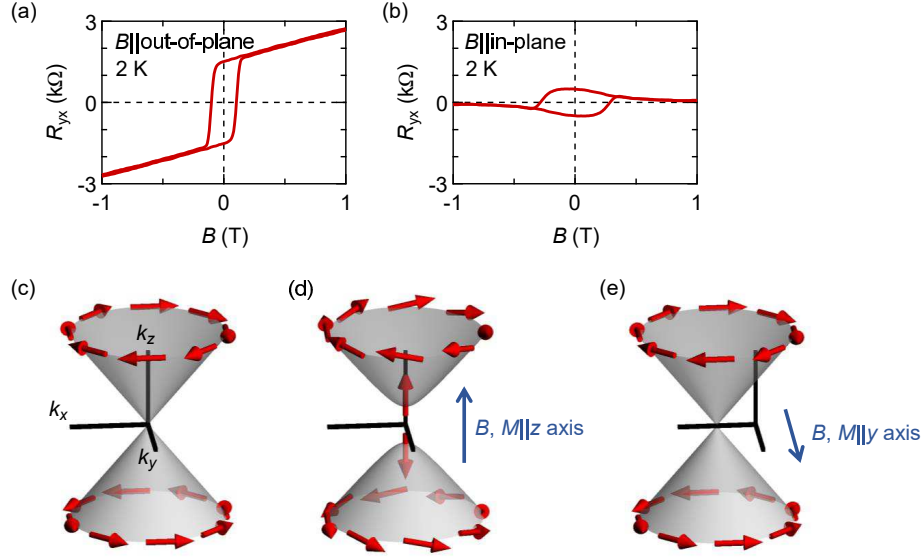


Fig. S2. (a) Magnetic field dependence of Hall resistance R_{yx} with $B||\text{out-of-plane}$. (b) Same as (a) with $B||\text{in-plane}$. R_{yx} is almost zero at and above 0.7 T, meaning $M||\text{in-plane}$. (c) Schematic diagram of the band structure without B and M . (d) with $B, M||z\text{-axis}$. (e) with $B, M||y\text{-axis}$.

SUPPLEMENTAL MATERIAL S3 | ESTIMATION OF HEATING BY CURRENT INJECTION

Figure S3 shows the estimation of heating by current injection. The resistance is decreased by heating as we apply larger current. By comparing with temperature dependence of R/R_0 measured with minimal current ($0.1 \mu\text{A}$), the sample temperature is estimated to increase from 2 K to 2.7 K when applying $1 \mu\text{A}$. Also, with $3 \mu\text{A}$, it increases from 2 K to 4.3 K. For most measurements except for the current dependence, we applied $\pm 1 \mu\text{A}$ to get enough S/N ratio but to make the heating effect as small as possible. This heating effect, combined with the decrease of signal at high temperature (top panel of Fig. 3(c) in the main text), results in the breakdown of the linear relationship between ΔR_{xx} and J at a higher current region in Fig. 1(k) in the main text.

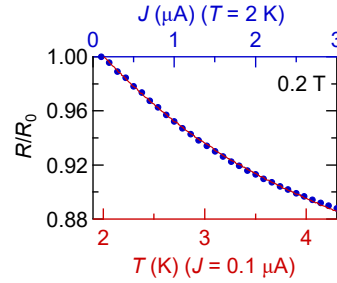


Fig. S3. The current dependence (at $T = 2 \text{ K}$) and temperature dependence (at $J = 0.1 \mu\text{A}$) of normalized resistance. The measurements were done at 0.2 T with $B||z\text{-axis}$.

SUPPLEMENTAL MATERIAL S4 | ESTIMATION OF CURIE TEMPERATURE

In Fig. S4, we show the magnetic field dependence of Hall resistance. The anomalous Hall effect and the coercive field decreases with the increase of temperature. From the temperature dependence of the anomalous Hall effect, we can estimate the T_C as $\sim 24 \text{ K}$.

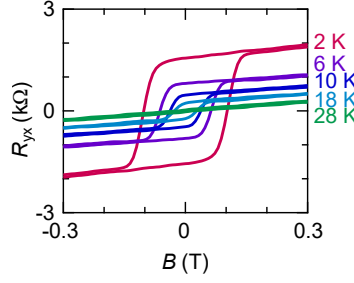


Fig. S4. Magnetic field $B||z$ -axis dependence of Hall resistance R_{yx} at selected temperatures.

SUPPLEMENTAL MATERIAL S5 | STRUCTURE DEPENDENCE OF UMR

Figure R5 shows the structure dependence of UMR for CBST/BST, BST/CBST, single-layer CBST and single-layer BST. Here, CBST/BST and BST/CBST are taken from Figs. 1(f) and 1(i) in the main text. In single-layer CBST, ΔR_{xx} takes a small finite value. Here, although the overall shape of the magnetic field dependence is the same as that in CBST/BST, the absolute value of the signal is about 10 times smaller. Since Cr is distributed over the whole film in CBST, both the top and bottom surfaces would exhibit finite UMR with an opposite sign, leading to the cancellation of the signal. Here, the observed smaller but finite signal probably originates from the difference in those environments. As for single-layer BST, on the other hand, no UMR signal is observed within the range of measurement error. This reconfirms the magnetic origin of UMR.

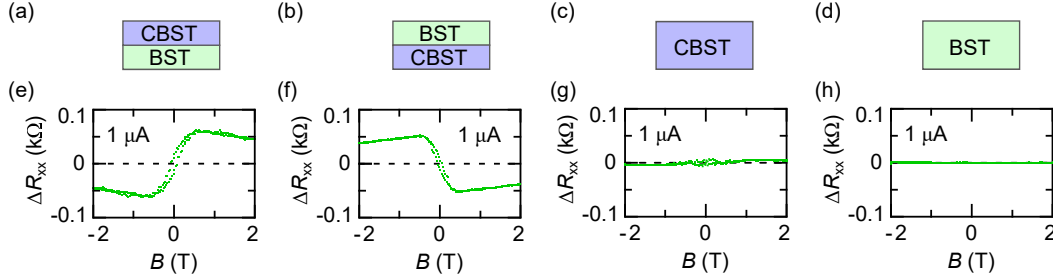


Fig. S5. (a)-(d) Schematic sample configurations for structure dependent characterization of UMR signal; CBST/BST (a), BST/CBST (b), CBST (c) and BST (d). The total thickness of each sample is fixed to 8 nm. (e)-(h) In-plane magnetic field dependence of ΔR_{xx} at $T = 2$ K.

SUPPLEMENTAL MATERIAL S6 | DERIVATION OF NONLINEAR CONDUCTION

Here, we derive the expression for the nonlinear Boltzmann transport equation using relaxation time approximation. When \mathbf{E} is large enough, we need to discuss the nonlinear resistance beyond linear response $\mathbf{J} = \sigma \mathbf{E}$.

First, we derive the relationship between \mathbf{J} and \mathbf{E} [S1]. We define the distribution function of electron as $g(\mathbf{r}, \mathbf{k}, t) = g(\mathbf{k})$. Here, we assume time-independent uniform electric field so that g is dependent only on \mathbf{k} . When $\mathbf{E} = 0$ (equilibrium), the distribution function is expressed by Fermi distribution function,

$$g^0(\mathbf{k}) = f(\mathbf{k}) = \frac{1}{e^{(\epsilon(\mathbf{k}) - \mu)/k_B T} + 1}. \quad (\text{S4})$$

We first consider the scattering of electron by impurity, phonon, electron-electron, magnon *etc.* In the relaxation time approximation, the electron is assumed to relax to equilibrium within the typical timescale of τ as follows,

$$\left(\frac{dg(\mathbf{k})}{dt} \right)_{\text{coll}} = -\frac{g(\mathbf{k}) - g^0(\mathbf{k})}{\tau(\mathbf{k})}. \quad (\text{S5})$$

Next, assuming equation (S5), we derive the nonlinear distribution function. Boltzmann equation is expressed as,

$$\frac{\partial g}{\partial t} + \mathbf{v} \cdot \frac{\partial g}{\partial \mathbf{r}} + \mathbf{F} \cdot \frac{1}{\hbar} \frac{\partial g}{\partial \mathbf{k}} = \left(\frac{dg(\mathbf{k})}{dt} \right)_{\text{coll}}. \quad (\text{S6})$$

In the steady state under uniform electric field,

$$\frac{\partial g}{\partial t} = 0, \quad \frac{\partial g}{\partial \mathbf{r}} = 0, \quad \mathbf{F} = -e\mathbf{E}, \quad (\text{S7})$$

so that the equation (S6) is expressed as,

$$-\frac{e\mathbf{E}}{\hbar} \cdot \frac{\partial g}{\partial \mathbf{k}} = -\frac{g - g^0}{\tau}. \quad (\text{S8})$$

Namely,

$$g = f + \frac{e\mathbf{E}\tau}{\hbar} \cdot \frac{\partial g}{\partial \mathbf{k}}. \quad (\text{S9})$$

In the following, we consider the case of $\mathbf{E} = (E_x, 0, 0)$ for simplicity. The linear approximation leads to the well-known relation [S1],

$$j_x = \sigma_{xx}^{(1)} E_x, \quad (\text{S10})$$

$$\sigma_{xx}^{(1)} = e^2 \int \frac{d\mathbf{k}}{4\pi^3} \tau(\mathbf{k}) v_x(\mathbf{k}) v_x(\mathbf{k}) \left(-\frac{\partial f}{\partial \epsilon} \right). \quad (\text{S11})$$

Expanding the formula up to E^2 term, *i.e.*,

$$g = f + \frac{eE\tau}{\hbar} \frac{\partial}{\partial k_x} \left(f + \frac{eE\tau}{\hbar} \frac{\partial f}{\partial k_x} \right) \quad (\text{S12})$$

$$= f + \frac{eE\tau}{\hbar} \frac{\partial f}{\partial k_x} + \left(\frac{eE\tau}{\hbar} \right)^2 \left(\frac{\partial^2 f}{\partial k_x^2} \right), \quad (\text{S13})$$

we obtain the non-linear conductivity,

$$j_x = \sigma_{xx}^{(1)} E_x + \sigma_{xx}^{(2)} E_x^2, \quad (\text{S14})$$

$$\sigma_{xx}^{(2)} = -\frac{e^3}{\hbar^2} \int \frac{d\mathbf{k}}{4\pi^3} (\tau(\mathbf{k}))^2 v_x(\mathbf{k}) \left(\frac{\partial^2 f}{\partial k_x^2} \right). \quad (\text{S15})$$

In order to make comparison between the theory and the measured resistance, we discuss the relationship between ΔR_{xx} and $\sigma_{xx}^{(2)}$. To the first order approximation of equation (S14), we get

$$V_x = \frac{A}{l} E_x = \frac{A}{l} \left(\frac{1}{\sigma_{xx}^{(1)}} j_x - \frac{\sigma_{xx}^{(2)}}{(\sigma_{xx}^{(1)})^3} j_x^2 \right). \quad (\text{S16})$$

Here, A and l is the cross-sectional area and length of the Hall bar, respectively. Thus, when we excite plus or minus dc current, the measured resistance is,

$$R_{xx}^+ = \frac{1}{l} \left(\frac{1}{\sigma_{xx}^{(1)}} - \frac{\sigma_{xx}^{(2)}}{(\sigma_{xx}^{(1)})^3} j_x \right), \quad (\text{S17})$$

$$R_{xx}^- = \frac{1}{l} \left(\frac{1}{\sigma_{xx}^{(1)}} + \frac{\sigma_{xx}^{(2)}}{(\sigma_{xx}^{(1)})^3} j_x \right), \quad (\text{S18})$$

$$R_{xx} = \frac{R_{xx}^+ + R_{xx}^-}{2} = \frac{1}{l} \left(\frac{1}{\sigma_{xx}^{(1)}} \right), \quad (\text{S19})$$

$$\Delta R_{xx} = R_{xx}^+ - R_{xx}^- = -\frac{1}{l} \left(\frac{2\sigma_{xx}^{(2)}}{(\sigma_{xx}^{(1)})^3} j_x \right). \quad (\text{S20})$$

In the following, we discuss the microscopic origin of ΔR_{xx} and UMR.

SUPPLEMENTAL MATERIAL S7 | MICROSCOPIC ORIGIN OF UMR

Here, we discuss the microscopic origin of $\sigma_{xx}^{(2)}$ in magnetic TI. For simplicity, we first consider the 1D Dirac dispersion. According to equation (S15) the origin of $\sigma_{xx}^{(2)}$ can be divided into,

- i). asymmetry between $+\mathbf{k}$ and $-\mathbf{k}$ in $v_x(\mathbf{k}) \left(\frac{\partial^2 f}{\partial k_x^2} \right)$,
- ii). asymmetry between $+\mathbf{k}$ and $-\mathbf{k}$ in $(\tau(\mathbf{k}))^2$.

In completely k -linear Dirac dispersion, the Dirac point and the whole dispersion shift to the k_x -direction under magnetic field and/or magnetization along the y -direction so that v_x is unchanged (Fig. S2e). However, in the surface state of $(\text{Bi}_{1-x}\text{Sb}_x)_2\text{Te}_3$, k^2 term and hexagonal warping (k^3 term) actually exist in addition to the k -linear term [S2]. Therefore, because of the contribution from i), $\sigma_{xx}^{(2)}$ can be finite and is expected to increase as the in-plane component of magnetization M_y increases. In reality, as shown in Fig. 3(a) in the main text, ΔR_{xx} decreases as a function of the magnetic field (> 1 T). Therefore, the relative contribution from i) seems to be small in the present case.

Next we discuss the contribution from ii). From the temperature dependence in Fig. 3(a) in the main text, we already know that UMR is related to magnetism. Therefore, it is natural for us to consider the scattering of electrons by magnetic excitations, or magnons. Here, we consider the interaction between the surface conduction electron composed of Bi, Sb and Te p orbital and the localized spin composed of Cr d orbital. When M is pointing along y direction, the localized spin is pointing in the $-y$ direction. Therefore, the angular momentum of magnon is $+1$. Here, by the conservation of angular momentum, the interaction Hamiltonian \mathcal{H}' is written as,

$$\mathcal{H}' \propto \sum_i \left(c_{i,\uparrow}^\dagger c_{i,\downarrow} b_i + c_{i,\downarrow}^\dagger c_{i,\uparrow} b_i^\dagger \right) \quad (\text{S21})$$

$$= \sum_{k,q} \left(c_{k+q,\uparrow}^\dagger c_{k,\downarrow} b_q + c_{k-q,\downarrow}^\dagger c_{k,\uparrow} b_q^\dagger \right). \quad (\text{S22})$$

Here, b^\dagger (b) and c^\dagger (c) are a creation (annihilation) operator of magnon and surface Dirac electron, respectively. The equation (S21) means that the interaction at sites i can have only two types of process. One process is $c_{i,\uparrow}^\dagger c_{i,\downarrow} b_i$ meaning that electron spin is changed from \downarrow ($s_y = -\frac{1}{2}$) to \uparrow ($s_y = \frac{1}{2}$) by the absorption of magnon. This is because of the conservation of angular momentum; $-\frac{1}{2} + (+1) = \frac{1}{2}$ (note that the angular momentum of magnon is $+1$). Another process is $c_{i,\downarrow}^\dagger c_{i,\uparrow} b_i^\dagger$ meaning that electron spin is reversed from \uparrow ($s_y = \frac{1}{2}$) to \downarrow ($s_y = -\frac{1}{2}$) by the emission of magnon ($\frac{1}{2} - (+1) = -\frac{1}{2}$). Because of the spin-momentum locking of TI, the electron absorbs magnon to move from left branch to right one, while it emits magnon to move from right branch to left one. Here, the related magnon wavenumber is about $2k_F$ because of the conservation of momentum. These processes are schematically shown in Fig. S6. Because of such asymmetry in inelastic scattering by magnon, we naively expect asymmetry between $+\mathbf{k}$ and $-\mathbf{k}$ in $(\tau(\mathbf{k}))^2$, which leads to the UMR.

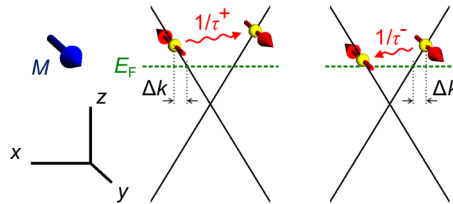


Fig. S6. Schematic pictures of asymmetric scattering of electron by magnon, where E_F is at the electron side. The Δk is measured from k_F (Fermi wavenumber).

SUPPLEMENTAL MATERIAL S8 | CALCULATION OF UMR IN 1D DIRAC DISPERSION

In the following, we derive the formula for ΔR_{xx} in 1D Dirac dispersion for the qualitative understanding of the magnon scattering process. There are many sources of scattering in crystal such as impurity, phonon, electron-electron

scattering. We assume that magnon scattering and these processes are completely independent of each other, then the relaxation time is written as

$$\frac{1}{\tau} = \frac{1}{\tau^{(0)}} + \frac{1}{\tau_{\text{mag}}}. \quad (\text{S23})$$

Here, $\tau^{(0)}$ is nonmagnetic scattering and τ_{mag} is scattering by magnon. Since the impurity scattering is dominant, $\tau^{(0)} \ll \tau_{\text{mag}}$ hold true in this case. Therefore, to the first order approximation, the relaxation time is expressed as,

$$\tau = \tau^{(0)} - \frac{(\tau^{(0)})^2}{\tau_{\text{mag}}}. \quad (\text{S24})$$

By substituting this to equation (S15), we obtain

$$\sigma_{xx}^{(2)} = -\frac{e^3}{\hbar^2} \int \frac{d\mathbf{k}}{4\pi^3} (\tau(\mathbf{k}))^2 v_x(\mathbf{k}) \left(\frac{\partial^2 f}{\partial k_x^2} \right) \quad (\text{S25})$$

$$= -\frac{e^3}{\hbar^2} \int \frac{d\mathbf{k}}{4\pi^3} \left((\tau^{(0)})^2 - \frac{2(\tau^{(0)})^3}{\tau_{\text{mag}}(\mathbf{k})} \right) v_x(\mathbf{k}) \left(\frac{\partial^2 f}{\partial k_x^2} \right) \quad (\text{S26})$$

$$= \frac{2(\tau^{(0)})^3 e^3}{\hbar^2} \int \frac{d\mathbf{k}}{4\pi^3} \frac{1}{\tau_{\text{mag}}(\mathbf{k})} v_x(\mathbf{k}) \left(\frac{\partial^2 f}{\partial k_x^2} \right). \quad (\text{S27})$$

Here, τ_{mag} can be expressed as

$$\frac{1}{\tau_{\text{mag}}(\mathbf{k})} = \int \frac{d\mathbf{k}'}{(2\pi)^3} W_{\text{mag}}(\mathbf{k}'|\mathbf{k})(1 - g(\mathbf{k}')), \quad (\text{S28})$$

$$W_{\text{mag}}(\mathbf{k}'|\mathbf{k}) = W_{\text{abs}}(\mathbf{k}', \sigma'; n_{-\mathbf{k}+\mathbf{k}'} - 1 | \mathbf{k}, \sigma; n_{-\mathbf{k}+\mathbf{k}'}) \quad (\text{S29})$$

$$+ W_{\text{emit}}(\mathbf{k}', \sigma'; n_{\mathbf{k}-\mathbf{k}'} + 1 | \mathbf{k}, \sigma; n_{\mathbf{k}-\mathbf{k}'}). \quad (\text{S30})$$

Here, W_{abs} and W_{emit} are scattering probability for the magnon absorption and emission process and $1 - g(\mathbf{k}')$ is the probability that the final destination of electron is unoccupied. \mathbf{k}, σ represent the electron wavenumber and spin, $n_{\mathbf{k}}$ corresponds to the number of magnon, respectively. Here, scattering probability is represented as,

$$W_{\text{abs}}(\mathbf{k}', \sigma'; n_{-\mathbf{k}+\mathbf{k}'} - 1 | \mathbf{k}, \sigma; n_{-\mathbf{k}+\mathbf{k}'}) = \frac{2\pi}{\hbar} |\langle \mathbf{k}', \sigma'; n_{-\mathbf{k}+\mathbf{k}'} - 1 | \mathcal{H}' | \mathbf{k}, \sigma; n_{-\mathbf{k}+\mathbf{k}'} \rangle|^2 \delta(\epsilon_{\mathbf{k}'} - \epsilon_{\mathbf{k}} - \hbar\omega_{-\mathbf{k}+\mathbf{k}'}) \quad (\text{S31})$$

$$= \frac{2\pi}{\hbar} n_{-\mathbf{k}+\mathbf{k}'} |\langle \sigma' | c_{\uparrow}^\dagger c_{\downarrow} | \sigma \rangle|^2 \delta(\epsilon_{\mathbf{k}'} - \epsilon_{\mathbf{k}} - \hbar\omega_{-\mathbf{k}+\mathbf{k}'}). \quad (\text{S32})$$

$$W_{\text{emit}}(\mathbf{k}', \sigma'; n_{\mathbf{k}-\mathbf{k}'} + 1 | \mathbf{k}, \sigma; n_{\mathbf{k}-\mathbf{k}'}) = \frac{2\pi}{\hbar} |\langle \mathbf{k}', \sigma'; n_{\mathbf{k}-\mathbf{k}'} + 1 | \mathcal{H}' | \mathbf{k}, \sigma; n_{\mathbf{k}-\mathbf{k}'} \rangle|^2 \delta(\epsilon_{\mathbf{k}'} - \epsilon_{\mathbf{k}} + \hbar\omega_{\mathbf{k}-\mathbf{k}'}) \quad (\text{S33})$$

$$= \frac{2\pi}{\hbar} (n_{\mathbf{k}-\mathbf{k}'} + 1) |\langle \sigma' | c_{\downarrow}^\dagger c_{\uparrow} | \sigma \rangle|^2 \delta(\epsilon_{\mathbf{k}'} - \epsilon_{\mathbf{k}} + \hbar\omega_{\mathbf{k}-\mathbf{k}'}), \quad (\text{S34})$$

Using equation (S28), we calculate τ_{mag}^+ , scattering of the electron from the left branch (displaced from k_F by Δk) to the right branch,

$$\frac{1}{\tau_{\text{mag}}^+(\Delta k)} \propto \frac{1}{e^{\beta\hbar\omega} - 1} \left(1 - \frac{1}{e^{\beta(\hbar\omega + \hbar v_F \Delta k)} + 1} \right). \quad (\text{S35})$$

Here, $\hbar\omega$ is an energy of magnon with $2k_F$ wavenumber. The first factor is the Bose factor corresponding to magnon population and the second factor the probability that the final destination is unoccupied. In a similar way, the relaxation time from right to left is expressed as,

$$\frac{1}{\tau_{\text{mag}}^-(\Delta k)} \propto \left(\frac{1}{e^{\beta\hbar\omega} - 1} + 1 \right) \left(1 - \frac{1}{e^{\beta(-\hbar\omega + \hbar v_F \Delta k)} + 1} \right). \quad (\text{S36})$$

Using these and equation (S27), we finally obtain the expression for nonlinear conduction in 1D Dirac dispersion,

$$\sigma_{xx}^{(2)} \propto (\tau^{(0)})^3 \int d\Delta k \left(\frac{1}{\tau_{\text{mag}}^+(\Delta k)} - \frac{1}{\tau_{\text{mag}}^-(\Delta k)} \right) \left(\frac{\partial^2 f}{\partial k_x^2}(\Delta k) \right). \quad (\text{S37})$$

Since $E = v_F k_x$, in 1D Dirac dispersion,

$$\frac{\partial^2 f}{\partial k_x^2} = v_F^2 \frac{\partial^2 f}{\partial E^2}. \quad (\text{S38})$$

Also, using equation (S11) we obtain,

$$\sigma_{xx}^{(1)} \propto \tau^{(0)}. \quad (\text{S39})$$

Therefore, from equation (S20) we get the expression for UMR in 1D Dirac dispersion,

$$\Delta R_{xx} \propto j_x \int d\Delta k \left(-\frac{1}{\tau_{\text{mag}}^+(\Delta k)} + \frac{1}{\tau_{\text{mag}}^-(\Delta k)} \right) \left(\frac{\partial^2 f}{\partial E^2}(\Delta k) \right), \quad (\text{S40})$$

which is the equation (2) in the main text.

In Fig. S7, we show the calculation result of equation (S40). We can see that $1/\tau_{\text{mag}}^-$ and $1/\tau_{\text{mag}}^+$ show clear deviation. The important point is that when Δk is positive, $1/\tau_{\text{mag}}^- > 1/\tau_{\text{mag}}^+$ and when it is negative, $1/\tau_{\text{mag}}^- < 1/\tau_{\text{mag}}^+$. Similarly, $\partial^2 f / \partial E^2$ also changes its sign depending on the sign of Δk . Therefore, the integrand of equation (S40) is positive for all Δk so that we get finite ΔR_{xx} .

We can derive exactly the same formula (S40) for the hole side in the case when E_F position is at the hole side (Fig. S7). Therefore, ΔR_{xx} gives the same sign for the electron and the hole side. Note that the above treatment of magnetic excitation is based on the spin wave approximation and hence that the theory is only applicable at low enough temperatures as compared with T_C [S1, S3]. Nevertheless, ΔR_{xx} is expected to diminish around and above T_C with vanishing M , in accord with the experimental result (Fig. 3(c) in the main text).

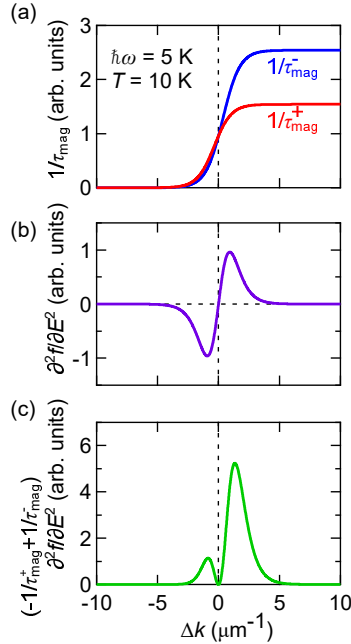


Fig. S7. (a) Δk dependence of $1/\tau_{\text{mag}}^-$ and $1/\tau_{\text{mag}}^+$. (b) Δk dependence of $\partial^2 f / \partial E^2$. (c) Δk dependence of the integrand of ΔR_{xx} . The calculation is done at $\hbar\omega = 5$ K and $T = 10$ K.

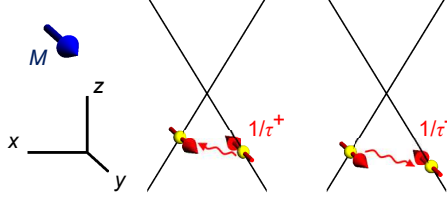


Fig. S8. Schematic pictures of asymmetric scattering at the hole side.

SUPPLEMENTAL MATERIAL S9 | CALCULATION OF UMR IN 2D DIRAC DISPERSION

Here, we expand the calculation of UMR in the 1D case to the 2D case. For simplicity, here we consider the linear dispersion again. The important difference from the 1D case is that the direction of spin is not fixed to the y -direction. We consider the scattering from the position α to θ as shown in Fig. S9. Here, spin eigenfunction at α is,

$$|\alpha\rangle = \sin \frac{\alpha}{2} |\uparrow\rangle + \cos \frac{\alpha}{2} |\downarrow\rangle. \quad (\text{S41})$$

Hence, the factors in equations (S34) and (S32) are expressed as,

$$|\langle\theta|c_{\uparrow}^{\dagger}c_{\downarrow}|\alpha\rangle|^2 = \cos^2 \frac{\alpha}{2} \times \sin^2 \frac{\theta}{2}, \quad (\text{S42})$$

$$|\langle\theta|c_{\downarrow}^{\dagger}c_{\uparrow}|\alpha\rangle|^2 = \sin^2 \frac{\alpha}{2} \times \cos^2 \frac{\theta}{2}. \quad (\text{S43})$$

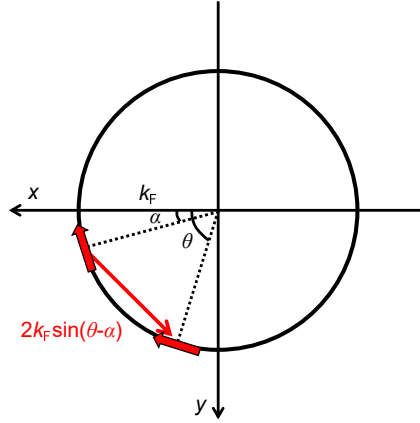


Fig. S9. Top view of the magnon scattering in 2D Dirac dispersion.

Therefore, when we define the integrand of equation (S28) as V_{mag} ,

$$V_{\text{mag}}(\theta, \alpha, \Delta k) = \cos^2 \frac{\alpha}{2} \sin^2 \frac{\theta}{2} V_{\text{mag}}^+(\alpha, \theta, \Delta k) + \sin^2 \frac{\alpha}{2} \cos^2 \frac{\theta}{2} V_{\text{mag}}^-(\alpha, \theta, \Delta k), \quad (\text{S44})$$

$$V_{\text{mag}}^+(\theta, \alpha, \Delta k) \propto \frac{1}{e^{\beta \hbar \omega} - 1} \left(1 - \frac{1}{e^{\beta(\hbar \omega + \hbar v_F \Delta k)} + 1} \right), \quad (\text{S45})$$

$$V_{\text{mag}}^-(\theta, \alpha, \Delta k) \propto \left(\frac{1}{e^{\beta \hbar \omega} - 1} + 1 \right) \left(1 - \frac{1}{e^{\beta(-\hbar \omega + \hbar v_F \Delta k)} + 1} \right). \quad (\text{S46})$$

Here, $\hbar\omega$ corresponds to the magnon energy with $2k_F \sin(\theta - \alpha)$ wavenumber. Using equation (S28), we get

$$\frac{1}{\tau_{\text{mag}}(\alpha, \Delta k)} = \int \frac{d\mathbf{k}'}{(2\pi)^3} V_{\text{mag}}(\theta, \alpha, \Delta k) \quad (\text{S47})$$

$$= \int \frac{dk'}{(2\pi)^3} \int d\theta k' V_{\text{mag}}(\theta, \alpha, \Delta k) \quad (\text{S48})$$

$$= \frac{k_F}{(2\pi)^3} \int d\theta V_{\text{mag}}(\theta, \alpha, \Delta k). \quad (\text{S49})$$

As for $v_x(\mathbf{k})$,

$$v_x(\alpha, \Delta k) = v_F \cos \alpha. \quad (\text{S50})$$

As for $\frac{\partial^2 f}{\partial k_x^2}$,

$$\frac{\partial^2 f}{\partial k_x^2}(\alpha, \Delta k) = \frac{\beta \hbar v_F}{k_F} \left(\frac{-P}{(P+1)^2} \right) \sin^2 \alpha + (\beta \hbar v_F)^2 \left(\frac{P(P-1)}{(P+1)^3} \right) \cos^2 \alpha \quad (\text{S51})$$

$$\simeq (\beta \hbar v_F)^2 \left(\frac{P(P-1)}{(P+1)^3} \right) \cos^2 \alpha, \quad (\text{S52})$$

$$P = e^{\beta \hbar v_F \Delta k}. \quad (\text{S53})$$

Here, in equation (S52), we can ignore the first term since $\beta \hbar v_F k_F \gg 1$ except for the immediate vicinity of the Dirac point. Summarizing these, we can calculate $\sigma_{xx}^{(2)}$ from equation (S27);

$$\sigma_{xx}^{(2)} \propto (\tau^{(0)})^3 k_F \int d\mathbf{k} \int d\theta \left[V_{\text{mag}}(\theta, \alpha, \Delta k) \left(\frac{\partial^2 f}{\partial k_x^2} \right) v_F \cos \alpha \right] \quad (\text{S54})$$

$$= (\tau^{(0)})^3 k_F^2 \int d\Delta k \int d\alpha \int d\theta \left[V_{\text{mag}}(\theta, \alpha, \Delta k) \left(\frac{\partial^2 f}{\partial k_x^2} \right) v_F \cos \alpha \right]. \quad (\text{S55})$$

Here, we ignored the anisotropy of $\tau^{(0)}$. Also, using equation (S11) we obtain,

$$\sigma_{xx}^{(1)} \propto \tau^{(0)} k_F. \quad (\text{S56})$$

Therefore, from equation (S20) we finally obtain the expression for the UMR of 2D Dirac dispersion,

$$\Delta R_{xx} \propto -\frac{j_x}{k_F} \int d\Delta k \int d\alpha \int d\theta \left[V_{\text{mag}}(\theta, \alpha, \Delta k) \left(\frac{\partial^2 f}{\partial k_x^2} \right) v_F \cos \alpha \right]. \quad (\text{S57})$$

In this expression, we can exclude the contribution from $\tau^{(0)}$ and hence discuss the temperature dependence and V_G dependence of UMR of magnon origin. The calculation results in Fig. 3(d) in the main text are obtained by the numerical calculation of equation (S57) assuming the simple circle Fermi surface of the Dirac cone.

SUPPLEMENTAL MATERIAL S10 | ORIGIN OF DEVIATION BETWEEN THE NUMERICAL CALCULATIONS AND THE EXPERIMENTAL RESULTS IN FIG. 3

Although the experimental results and numerical calculations give qualitative consistency, there is still quantitative deviation between them. The followings are the main causes of the deviation.

1. Relaxation time approximation

To calculate the scattering term at the right-hand side of Boltzmann equation (S6) in the Supplemental Material S5, we used the relaxation time approximation so that

$$\left(\frac{dg(\mathbf{k})}{dt} \right)_{\text{coll}} = -\frac{g(\mathbf{k}) - g^0(\mathbf{k})}{\tau(\mathbf{k})}. \quad (\text{S58})$$

For a more serious calculation, it should be replaced by

$$\left(\frac{dg(\mathbf{k})}{dt}\right)_{\text{coll}} = - \int \frac{d\mathbf{k}'}{(2\pi)^3} [W(\mathbf{k}|\mathbf{k}')g(\mathbf{k})(1-g(\mathbf{k}')) - W(\mathbf{k}'|\mathbf{k})g(\mathbf{k}')(1-g(\mathbf{k}))], \quad (\text{S59})$$

where $W(\mathbf{k}'|\mathbf{k})$ is the scattering probability from \mathbf{k} to \mathbf{k}' [1]. Since it is very difficult to carry out the calculation with equation (S59), we use relaxation time approximation in numerical calculation.

2. Spin wave approximation

Spin wave approximation is used in Supplemental Material S7 and S8 [3]. As mentioned in Supplemental Material S8, magnetic excitation is well-defined only at sufficiently low temperature than T_C , therefore the theoretical calculation shows deviation at high temperatures.

3. Simplified band dispersion

For the sake of simplicity, we assumed a linear Dirac band dispersion. In fact, k^2 term and hexagonal warping (k^3 term) actually exist in the band dispersion in addition to the k -linear term [2]. Although the linear Dirac band captures the essence of UMR, this also results in the deviation in the theoretical calculation.

4. Estimation of the spin wave gap

We put Zeeman term ($g\mu_B B$) as a gap energy of magnon in the calculation. Since magnons with finite wavenumber is the source of scattering, we should take into account the band dispersion of magnon. To derive the band dispersion of magnon, however, it is necessary to estimate of the magnitude of the exchange interaction J , as well as to take into account the dipole-dipole interaction, which makes the calculation more complicated. Hence, as a first step, we considered only the Zeeman term this time.

There is deviation between in the experimental results and the theoretical calculations because of some simplifications and approximations as described above. The essence of UMR is, however, captured by the theoretical formula; the change of the energy scale (peak position of ΔR_{xx}) as a function of the magnetic field is well-reproduced in Fig. 3 in the main text. Improvement of the theoretical calculation without those simplifications and approximations remains as a future issue.

* yasuda@cmr.t.u-tokyo.ac.jp

[S1] N. W. Ashcroft, and N. D. Mermin, *Solid State Physics* (Saunders College, 1976).

[S2] H. Zhang, C. X. Liu, X. L. Qi, X. Dai, Z. Fang, and S. C. Zhang, *Nat. Phys.* **5**, 438 (2009).

[S3] T. Holstein, and H. Primakoff, *Phys. Rev.* **58**, 1098 (1940).